

Sharing Mobilized Energy Storage for Temporal-spatial Coordination of Transportation and Power Systems

Yuhang Ding, Xinjiang Chen, *Student Member, IEEE*, Guangchun Ruan, *Member, IEEE*, Gengyin Li, *Member, IEEE*, Ming Zhou, *Senior Member, IEEE*, Jiang Dai, and Jianxiao Wang, *Senior Member, IEEE*

Abstract—Mobilized energy storage (MES) can provide a variety of services for power systems, including peak shaving, frequency regulation, and congestion alleviation. In this paper, we develop an MES sharing approach based on temporal-spatial network (TSN) toward systemwide temporal-spatial flexibility enhancement, specifically in which the heavy-duty vehicles can exchange batteries at the energy storage stations connected with power grids. To achieve the temporal-spatial coordination of transportation and power systems, we propose a coordinated scheduling model. A decentralized algorithm based on the improved optimality condition decomposition (OCD) algorithm is proposed to address the information asymmetry between transportation and power systems while enhancing computational efficiency. Case studies based on IEEE 30-/118-bus and transportation systems demonstrate that MESs using the proposed approach can significantly improve the utilization of batteries while reducing operating costs by over 40% compared with stationary energy storages (SESs).

Index Terms—Mobilized energy storage, optimality condition decomposition, storage sharing, coordination of transportation and power systems, temporal-spatial network.

I. INTRODUCTION

THE increasing contribution of renewable energy in the power systems has resulted in a reduction in energy costs and air pollution [1]. However, the variabilities and uncertainties of renewable energy present a significant challenge to the economic and reliable operation of power systems [2]–[5]. Energy storage system (ESS) is a key technology to promote a high penetration of renewable energy, which can mitigate fluctuations, improve power quality, and reduce wind and photovoltaic curtailment [6]. For example, three largest utilities in California, USA, were required to procure 1325 MW of ESSs for power supply across their power system that has high penetration of renewable energy [7]. In 2023, the global battery energy storage capacity increased by 42 GW [8]. In China, 5%–20% of the capacity of ESSs in a connected renewable station is required to be provided for the power grid [9].

Stationary energy storages (SESs) can achieve energy shift over a time horizon. For SESs, operators need to plan for energy storage capacity and locations. However, the uncertainty of renewable energy impedes the achievement of optimal results in SES planning [10]. Moreover, SESs rely on large-capacity, long-distance transmission lines. The aforementioned issues may lead to a deficiency in energy storage and the wastage of resources.

Therefore, mobilized energy storages (MESs) have received extensive attention [11]. Compared with SESs, MESs can cope with the uncertainty of renewable energy and improve resource utilization. Furthermore, the mobility of MESs makes them highly useful in auxiliary services such as peak shaving and congestion management [12]. In recent years, the commercial deployment of MESs has increased as the cost of utility-scale batteries continues to fall [13]–[15]. China Southern Power Grid (CSG) has developed the first high-voltage MES station with 6 MW power and 7.2 MWh capacity in China. Nomad provides MESs based on renewable energy to various industries in USA [16]. Research on large utility-scale MESs has broad prospects.

Maximizing the potential of MESs requires coordination between the transportation and power systems. In existing research, transportation and power system coordination mainly

Manuscript received: December 10, 2023; revised: April 1, 2024; accepted: August 5, 2024. Date of CrossCheck: August 5, 2024. Date of online publication: September 5, 2024.

This work was supported by National Natural Science Foundation of China (No. 52277092) and Chinese Association of Science and Technology Young Elite Scientists Sponsorship Program (No. YESS20210227).

This article is distributed under the terms of the Creative Commons Attribution 4.0 International License (<http://creativecommons.org/licenses/by/4.0/>).

Y. Ding, G. Li, and M. Zhou are with State Key Laboratory of Alternate Electrical Power System with Renewable Energy Sources, North China Electric Power University, Beijing 102206, China, and Y. Ding is also with State Grid Hangzhou Lin'an District Power Supply Company, Hangzhou 311399, China (e-mail: dingyuhang1208@163.com; ligy@ncepu.edu.cn; zhouting@ncepu.edu.cn).

X. Chen is with Department of Industrial Engineering and Management, College of Engineering, Peking University, Beijing 100871, China (e-mail: xinjiangchen@stu.pku.edu.cn).

G. Ruan is with the Laboratory for Information and Decision Systems, Massachusetts Institute of Technology, Cambridge, MA 02139, USA (e-mail: rgethu@163.com).

J. Dai is with Power Dispatching and Control Center, Guizhou Power Grid Company, Guiyang 550002, China (e-mail: 553097875@qq.com).

J. Wang (corresponding author) is with National Engineering Laboratory for Big Data Analysis and Applications, Peking University, Beijing 100871, China (e-mail: wang-jx@pku.edu.cn).

DOI: 10.35833/MPCE.2023.000976



focuses on two key areas: the coordination optimization of transportation and power system flows [17] and the vehicle routing problem (VRP). The VRP is stated as “Given a depot and several vehicles and customers, how can the vehicles be efficiently scheduled to service all customers while minimizing the total traveling cost [18]?” According to existing research, there are primarily two types of VRP models: the sliding-window-based model (SWBM) [19] and the temporal-spatial network (TSN) [20]. Coordinating the limited MESSs and power systems is a typical VRP.

Some studies focus on the integrated operation of MESSs with the power systems. In [21], a distribution system scheduling model integrating MESSs is proposed, which ignores traffic medium and only considers the transportation time between buses. In [22], a battery-based energy transportation system integrated unit commitment problem is proposed. The Lagrangian decomposition algorithm is then proposed in [23] as a solution to the problem, and the uncertainty of wind power and the system is considered in [24]. In [25], a bi-level optimization model is proposed for the economic operation of MESSs in integrated transportation and power systems. The upper level focuses on the daily operation plan of MESSs to maximize system revenue, while the lower level optimizes transportation routes. In [26], a two-stage stochastic management scheme is introduced to minimize expected operating costs. The first stage models and optimizes vehicle routing of MESSs, while the second stage adjusts charging and discharging behavior in response to uncertainty. Some studies also discuss the potential of large-scale aggregated electric vehicles (EVs) as MESSs [27], [28]. However, EVs are affected by random behavior of drivers compared with MESSs.

Moreover, some studies focus on the planning of MESSs. In [29], a two-stage optimization model is proposed: the first stage optimizes MES investments, and the second stage re-routes MESSs under extreme conditions. In [30], a two-step allocation model is proposed: the first step selects ESS locations under normal conditions, and the second step uses a robust optimization model to optimize ESS allocation under extreme conditions. However, the planning problem considering MESSs is generally a two-stage mixed-integer linear programming (MILP) problem with binary recourse decision-making, which requires high computational performance.

For the commercial value of MESSs, an optimization model is proposed in [31] to demonstrate the feasibility of temporal-spatial arbitrage of MESSs in California, USA. In [32] and [33], the concept of battery transport and logistics is proposed. These batteries are charged in the renewable energy plants and profit from railway transportation between power plants and cities. However, these studies do not consider coordinated scheduling with the power systems.

Most studies consider the energy storage and MES vehicles to be a dependent entity. This approach weakens the flexibility of MESSs over the time horizon, making MESSs less economical than SESs in most cases. Moreover, many studies currently focus on the impact of small-scale energy storage on distribution networks. While with the development of MESSs, it is necessary to ensure the economic opera-

tion of large utility-scale MESSs. As a major characteristic of battery energy storage, modularity makes the size of ESSs highly scalable. In other words, operators can easily assemble multiple standard storage units to tailor the desired storage capacity [34], [35].

Inspired by [32] and [33], we propose an MES sharing approach that decouples energy storage from transportation vehicles. This approach optimally exploits the spatial flexibility of MESSs while minimizing the loss of temporal flexibility. Subsequently, a coordinated scheduling model that integrates large utility-scale MESSs based on the MES sharing approach is established in this paper. A comparison between the proposed model and those in the previous references is given in Table I.

TABLE I
COMPARISON OF PROPOSED MODEL AND THOSE IN RELATED REFERENCES

Model	Objective	MES approach	Stage	Grid	TM
Ref. [21]	Economic	Integrated	Scheduling	DN	SWBM
Refs. [22]-[24]	Economic	Integrated	Scheduling	TN	TSN
Ref. [25]	Economic	Integrated	Scheduling	DN	SWBM
Ref. [29]	Resilience	Integrated	Planning	DN	SWBM
Ref. [30]	Resilience	Integrated	Planning	DN	SWBM
Refs. [32], [33]	Economic	Decoupled	Scheduling		SWBM
Proposed	Economic	Decoupled	Scheduling	TN	TSN

Note: DN stands for the distributed network; TN stands for the transmission network; and TM stands for the transportation model.

The contributions of this paper are summarized as follows.

1) A MES sharing approach based on TSN is proposed for power system optimization. This approach realizes the coupling of power and transportation systems through energy storage capacity exchange.

2) A coordinated scheduling model is proposed to achieve the temporal-spatial coordination of transportation and power systems. The transportation system is used to transfer large utility-scale energy storage, aiming to minimize generation and transportation costs.

3) To address the information asymmetry in transportation and power systems, a decentralized algorithm based on the improved optimality condition decomposition (OCD) algorithm is proposed to decompose the coordinated problem into two subproblems for decoupled transportation and power systems.

The rest of this paper is organized as follows. Section II presents the framework of transportation and power systems. Section III describes the model of the proposed MES sharing approach. Section IV proposes a coordinated scheduling model for transportation and power systems. Section V describes the decentralized algorithm based on improved OCD algorithm for the coordinated scheduling model. Case studies are tested in Section VI. Section VII concludes this paper.

II. FRAMEWORK OF TRANSPORTATION AND POWER SYSTEMS

The framework of transportation and power systems in Fig. 1 aims to minimize the operating cost of the coupled

system. In this system, we propose an MES sharing approach. The energy storage and MES vehicles can be decoupled, with MES vehicles dynamically changing the spatial distribution of energy storage through battery transportation. These vehicles do not stop at energy storage stations during charging and discharging. Therefore, energy storage can be flexibly allocated during the scheduling period to improve fault tolerance during the planning period. In addition to high-voltage transmission grids, MESs offer an alternative means of transporting power resources in remote areas. MES vehicles can place empty batteries in resource-rich areas to utilize curtailment energy during off-peak hours. The fully charged batteries can be placed in load centers and heavily congested areas during peak hours. MESs can also provide temporary electricity for areas where power facilities are being built. Moreover, MESs can temporarily support the operation of power systems under fault conditions.

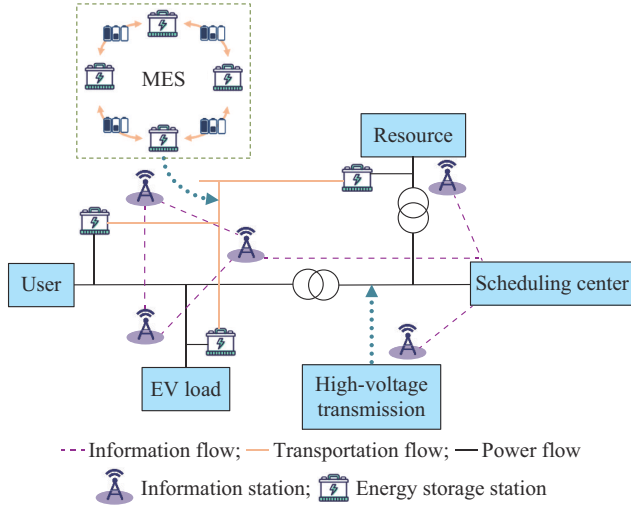


Fig. 1. Framework of transportation and power systems.

The MES sharing approach can significantly improve the asset utilization of energy storage. The expansion of energy storage capacity presents a challenge in the planning of large-scale energy storage in the future. The proposed approach can redistribute the location of energy storage devices during operation, reducing the risk associated with the planning stage.

To highlight the research focus, the following assumptions are made for the transportation system.

- 1) The transportation system operator is assumed to be a railway operator. The trains only transfer energy storage, and no other goods are transferred.
- 2) The specific profit model of transportation system operators is ignored.
- 3) The congestion of the transportation system is ignored, and the transportation time between different energy storage stations is the same.
- 4) Only the transportation cost of the train is considered as a linear function of time.

III. MODEL OF PROPOSED MES SHARING APPROACH

In this paper, the model of proposed MES sharing ap-

proach is proposed, which considers the battery energy storage capacity exchange between energy storage stations and trains. Batteries that can increase or decrease energy storage capacity of energy storage stations are transported by transportation systems based on railways. The transportation system and power grid overlap geographically, interacting through energy storage stations. According to the load and transmission demand, the battery energy storage capacity of energy storage stations can be redistributed by the transportation system. The key to this model is how to capture the dynamic and energy states of MESs.

A. TSN Model

TSN is a commonly used tool for describing VRP. We use a TSN to capture the dynamic states of MESs, which effectively balances modeling difficulty, solution accuracy, and computation time [22]. The 0-1 variable $L_{ij,v,t}$ is used to represent the states of train v within time span t in the transportation system. ij represents the arc from node i to node j . When $i \neq j$, the train is moving on arc ij . When $i = j$, the train is connected to node i . The constraints are shown as follows:

$$\sum_{ij \in \Phi^N} L_{ij,v,t} = 1 \quad \forall i, \forall v, \forall t \quad (1)$$

$$\sum_{ij \in \Phi^{N^+}} L_{ij,v,t+1} - \sum_{ji \in \Phi^{N^-}} L_{ji,v,t} = 0 \quad \forall i, \forall v, t = 1, 2, \dots, T-1 \quad (2)$$

$$\sum_{ij \in \Phi^{N^+}} L_{ij,v,1} - L_{ji,v,0} = 0 \quad \forall i, \forall v \quad (3)$$

$$L_{ji,v,T} - \sum_{ij \in \Phi^{N^-}} L_{ij,v,T-1} = 0 \quad \forall i, \forall v \quad (4)$$

where $L_{ij,v,0}$ and $L_{ij,v,T}$ are the initial and final states of train v in arc ij , respectively; Φ^N is the set of arcs; T is the last time span; and Φ^{N^+} and Φ^{N^-} are the sets of arcs that start and end from energy storage station i , respectively.

Equation (1) indicates that each train v can only be on one arc during time span t . Equation (2) indicates the continuity of MES routines. Equations (3) and (4) represent the start and end states of each train v , respectively.

B. Model of Battery Energy Storage Capacity Exchange

The key to the energy states of MESs in this model is how to capture the battery energy storage capacity exchange between energy storage stations and trains. Due to the modularity of battery, it is believed that energy storage stations and trains can exchange optimal capacity without being limited by integration. Therefore, the battery energy storage capacity is defined as a continuous variable to reduce the computational complexity. The battery energy storage capacity limits the maximum energy and power. This approach is suitable for day-ahead optimization or emergency scenarios. In this subsection, energy storage stations and trains are modeled as follows.

1) Model of Energy Storage Stations

$$0 \leq C_{i,t}^+ \leq C_{\max} \quad \forall i, \forall t \quad (5)$$

$$0 \leq C_{i,t}^- \leq C_{\max} \quad \forall i, \forall t \quad (6)$$

$$0 \leq C_{i,t} \leq C_{\max} \quad \forall i, \forall t \quad (7)$$

$$C_{i,t} = C_{i,t-1} + C_{i,t}^+ - C_{i,t}^- \quad \forall i, \forall t \quad (8)$$

where $C_{i,t}$ is the battery energy storage capacity of energy storage station i at time t ; $C_{i,t}^+$ and $C_{i,t}^-$ are the increase and decrease of battery energy storage capacity of energy storage station i at time t , respectively; and C_{\max} is the maximum battery energy storage capacity of energy storage stations.

Formulas (5)-(8) show the constraints of battery energy storage capacity in energy storage stations. Constraints (5) and (6) represent that the increase and decrease of battery energy storage capacity of energy storage station are limited by the maximum battery energy storage capacity of energy storage station. Constraint (7) represents the battery energy storage capacity limitation of energy storage stations. Constraint (8) shows that the battery energy storage capacity of energy storage station is related to the increase and decrease of battery energy storage capacity during a time span. And (8) also ensures that the increase and decrease of battery energy storage capacity are limited by the energy storage station capacity.

$$0 \leq E_{i,t}^+ \leq \min \{E_{\max}, \sigma C_{i,t}^+\} \quad \forall i, \forall t \quad (9)$$

$$0 \leq E_{i,t}^- \leq \min \{E_{\max}, \sigma C_{i,t}^-\} \quad \forall i, \forall t \quad (10)$$

$$0 \leq E_{i,t} \leq \sigma C_{i,t} \quad \forall i, \forall t \quad (11)$$

$$E_{i,t} = \underbrace{E_{i,t-1} + E_{i,t}^+ - E_{i,t}^-}_{\text{The first part}} + \underbrace{\eta P_{i,t-1}^{cha} - P_{i,t-1}^{dis} / \eta}_{\text{The second part}} \quad \forall i, \forall t \quad (12)$$

where $E_{i,t}$ is the energy of energy storage station i at time t ; $E_{i,t}^+$ and $E_{i,t}^-$ are the energy increase and decrease of energy storage station i at time t , respectively; E_{\max} is the maximum energy of energy storage stations; σ is a constant for the minimum charging and discharging time of a 1 MWh battery; η is the charging and discharging efficiency; and $P_{i,t}^{cha}$ and $P_{i,t}^{dis}$ are the charging and discharging power of energy storage station i at time t , respectively.

Formulas (9)-(12) show the energy constraints of energy storage stations. Constraints (9) and (10) represent the energy increase and decrease of the energy storage station, which are limited by the increase and decrease of battery energy storage capacity and the maximum energy of energy storage stations. Constraint (11) shows that the energy of energy storage stations is limited by the battery energy storage capacity of energy storage stations. Constraint (12) shows that the battery energy storage capacity of the energy storage station is related to the energy increase and decrease and the charging and discharging power during a time span. The first part of (12) represents the energy change caused by loading and unloading batteries at the energy storage station. The second part of (12) represents the energy change caused by the charging and discharging of the energy storage station.

$$0 \leq P_{i,t}^{cha} \leq \min \{C_{i,t}, \alpha_{i,t} C_{\max}\} \quad \forall i, \forall t \quad (13)$$

$$0 \leq P_{i,t}^{dis} \leq \min \{C_{i,t}, \beta_{i,t} C_{\max}\} \quad \forall i, \forall t \quad (14)$$

$$\alpha_{i,t} + \beta_{i,t} \leq 1 \quad \forall i, \forall t \quad (15)$$

where $\alpha_{i,t}$ and $\beta_{i,t}$ are the charging and discharging indices of the energy storage station, respectively.

Formulas (13)-(15) show the constraints of charging and

discharging power limitations of energy storage stations. The maximum charging and discharging power depends on the battery energy storage capacity of the energy storage station.

In this model, the energy storage station cannot charge and discharge simultaneously.

2) Model of Trains

$$0 \leq c_{i,v,t}^- \leq L_{ii,v,t} c_{\max} \quad \forall i, \forall v, \forall t \quad (16)$$

$$0 \leq c_{i,v,t}^+ \leq L_{ii,v,t} c_{\max} \quad \forall i, \forall v, \forall t \quad (17)$$

$$0 \leq c_{v,t} \leq c_{\max} \quad \forall v, \forall t \quad (18)$$

$$c_{v,t} = c_{v,t-1} + \sum_{i \in \Phi^s} c_{i,v,t}^+ - \sum_{i \in \Phi^s} c_{i,v,t}^- \quad \forall i, \forall v, \forall t \quad (19)$$

$$0 \leq e_{i,v,t}^- \leq \min \{L_{ii,v,t} e_{\max}, \sigma c_{i,v,t}^-\} \quad \forall i, \forall v, \forall t \quad (20)$$

$$0 \leq e_{i,v,t}^+ \leq \min \{L_{ii,v,t} e_{\max}, \sigma c_{i,v,t}^+\} \quad \forall i, \forall v, \forall t \quad (21)$$

$$0 \leq e_{v,t} \leq \sigma c_{\max} \quad \forall v, \forall t \quad (22)$$

$$e_{v,t} = e_{v,t-1} + \sum_{i \in \Phi^s} e_{i,v,t}^+ - \sum_{i \in \Phi^s} e_{i,v,t}^- \quad \forall i, \forall v, \forall t \quad (23)$$

where $c_{v,t}$ is the battery energy storage capacity of train v at time t ; $c_{i,v,t}^+$ and $c_{i,v,t}^-$ are the increase and decrease of battery energy storage capacity of train v at energy storage station i at time t , respectively; c_{\max} is the maximum battery energy storage capacity of trains; $e_{v,t}$ is the energy of train v at time t ; $e_{i,v,t}^+$ and $e_{i,v,t}^-$ are the energy increase and decrease of train v at energy storage station i at time t , respectively; e_{\max} is the maximum energy of trains; Φ^s is the set of energy storage station arcs in a TSN; and $L_{ii,v,t}$ indicates that the train is connected to energy storage station i that allows the train to interact with the energy storage station.

Formulas (16)-(23) show the battery energy storage capacity and energy constraints of the train, which are the same as those of the energy storage station.

$$\begin{cases} E_{i,t}^+ = \sum_{v \in \Phi^V} e_{i,v,t}^- \\ E_{i,t}^- = \sum_{v \in \Phi^V} e_{i,v,t}^+ \end{cases} \quad \forall i, \forall v, \forall t \quad (24)$$

$$\begin{cases} C_{i,t}^+ = \sum_{v \in \Phi^V} c_{i,v,t}^- \\ C_{i,t}^- = \sum_{v \in \Phi^V} c_{i,v,t}^+ \end{cases} \quad \forall i, v, t \quad (25)$$

where Φ^V is the set of trains.

Formulas (24) and (25) are the train and energy storage station interaction constraints.

In this model, $e_{i,v,t}^+$, $e_{i,v,t}^-$, $c_{i,v,t}^+$ and $c_{i,v,t}^-$ are the key variables that connect the train and the power grid.

IV. COORDINATED SCHEDULING MODEL FOR TRANSPORTATION AND POWER SYSTEMS

According to the model for proposed MES sharing approach in Section III, we propose a coordinated scheduling model for transportation and power systems, which focuses on the large utility-scale energy storage. A transmission system is adopted as the power system model in the paper. Therefore, a unit commitment model is adopted to describe

the power system.

A. Objective Function

The coordinated scheduling model aims to minimize the operating cost of the transportation and power systems. It optimizes the unit output, charging and discharging power of energy storage stations, and route of trains as follows:

$$\min \left\{ \sum_{t \in \Phi^T} \sum_{g \in \Phi^G} (C_g P_{g,t}^G + C_g^{SU} y_{g,t} + C_g^{SD} z_{g,t}) + \sum_{t \in \Phi^V} \sum_{v \in \Phi^V} \sum_{ij \in \Phi^P} C_{ij} L_{ij,v,t} \right\} \quad (26)$$

where $P_{g,t}^G$ is the power of thermal unit g at time t ; $y_{g,t}$ and $z_{g,t}$ are the start-up and shut-down indicators of thermal unit g at time t , respectively; C_g is the operating cost of thermal unit g ; C_g^{SU} and C_g^{SD} are the start-up and shut-down costs of thermal unit g , respectively; C_{ij} is the transportation cost of a train in arc ij ; Φ^T is the set of time spans; Φ^G is the set of thermal units; Φ^V is the set of MES trains; and Φ^P is the set of transportation arcs in a TSN.

In (26), the first part is the cost of thermal units, including the operating cost, start-up cost, and shut-down cost. The second part is the transportation cost.

B. Constraints

1) Constraints of Power System

$$x_{g,t} P_{g,\min}^G \leq P_{g,t}^G \leq x_{g,t} P_{g,\max}^G \quad \forall g, \forall t \quad (27)$$

$$y_{g,t} + z_{g,t} \leq 1 \quad \forall g, \forall t \quad (28)$$

$$y_{g,t} - z_{g,t} = x_{g,t} - x_{g,t-1} \quad \forall g, \forall t \quad (29)$$

$$P_{g,t}^G - P_{g,t-1}^G \leq L_t \cdot UR_{g,t} \quad \forall g, \forall t \quad (30)$$

$$P_{g,t}^G - P_{g,t-1}^G \geq -L_t \cdot DR_{g,t} \quad \forall g, \forall t \quad (31)$$

$$\sum_{\tau=t}^{t+T_{g,\min}^{on}-1} x_{g,\tau} \geq T_{g,\min}^{on} y_{g,t} \quad \forall g, \forall t \quad (32)$$

$$\sum_{\tau=t}^{t+T_{g,\min}^{off}-1} (1 - x_{g,\tau}) \geq T_{g,\min}^{off} z_{g,t} \quad \forall g, \forall t \quad (33)$$

$$0 \leq P_{r,t}^R \leq P_{r,\max}^R \quad \forall r, \forall t \quad (34)$$

$$\sum_{g \in \Phi^G} P_{g,t}^G + \sum_{r \in \Phi^R} P_{r,t}^R = \sum_{b \in \Phi^B} P_{b,t}^D + \sum_{i \in \Phi^S} (P_{i,t}^{cha} - P_{i,t}^{dis}) \quad (35)$$

$$-P_{l,\max}^L \leq F_{l-g} P_{g,t}^G + F_{l-r} P_{r,t}^R - F_{l-b} P_{b,t}^D - F_{l-i} (P_{i,t}^{cha} - P_{i,t}^{dis}) \leq P_{l,\max}^L \quad (36)$$

where $x_{g,t}$ is the operating state of thermal unit g at time t ; $P_{g,\max}^G$ and $P_{g,\min}^G$ are the maximum and minimum power of thermal unit g , respectively; L_t is the length of interval t ; $UR_{g,t}$ and $DR_{g,t}$ are the ramp-up and ramp-down rate limits of thermal unit g at time t , respectively; $T_{g,\min}^{on}$ and $T_{g,\min}^{off}$ are the minimum on and off times of thermal unit g , respectively; $P_{r,t}^R$ is the power of renewable energy unit r at time t ; $P_{r,\max}^R$ is the predicted maximum power of renewable energy unit r ; $P_{b,t}^D$ is the load of bus b at time t ; $P_{l,\max}^L$ is the maximum transmission capacity; F_{l-b} is the distribution factor of branch l to load bus b ; Φ^R is the set of renewable energy

units; and Φ^B is the set of load buses.

Formula (27) gives the upper and lower bounds of the output of thermal power units. Formulas (28) and (29) are the start-up and shut-down constraints of thermal power units. Formulas (30) and (31) are the ramp-up and ramp-down capability constraints of thermal power units. Formulas (32) and (33) are the minimum start-up and shut-down time constraints of thermal power units. Formula (34) is the output constraint of renewable energy units. Formulas (35) and (36) are the system balance and power flow constraints.

2) Constraints of MESs

The constraints of MESs consist of (1)-(25). Formulas (1)-(4) depict the movement of trains in the transportation system. Formulas (5)-(25) depict the battery energy storage capacity exchange between energy storage stations and trains.

This coordinated scheduling model is adopted to demonstrate the feasibility of the proposed MES sharing approach. The proposed approach can adapt to other topologies, but the computational performance may change. If it is implemented in a distribution system, the relevant constraints must be considered. This could be further explored in future research.

V. DECENTRALIZED ALGORITHM BASED ON IMPROVED OCD ALGORITHM

In practice, realizing the coordinated scheduling of the transportation and power systems requires the operators of both systems to submit detailed information to a central coordinator. However, transportation and power systems belong to different agencies in most areas. Therefore, a decentralized algorithm based on the improved OCD algorithm is proposed to decompose the coordinated scheduling problem into two subproblems [36]. The proposed coordinated scheduling model in Section IV is an MILP model with a large number of 0-1 variables, which results in a slow solution. The proposed algorithm can also improve the computational efficiency. The key to the proposed algorithm is to find the coupling variables and constraints of the two subproblems.

A. Decision-making Framework

The decision-making framework of the decomposed problem is shown in Fig. 2. The route of the train is determined in the transportation layer. The power demand and unit output for each time span are determined in the power layer. Additionally, the interaction between the transportation and power systems is achieved through the increase or decrease of batteries at the energy storage stations by trains. The operators of the two systems coordinate with each other through boundary information.

In existing studies, such coordination is achievable by a technique called optimal condition decomposition, which is essentially a modified version of Lagrangian relaxation. Based on the decomposition of coupling constraints, the proposed algorithm decomposes the coordinated scheduling problem into two subproblems and iteratively updates the boundary information until convergence is achieved. In the following subsections, the coupling constraint between the two subproblems will be fully discussed.

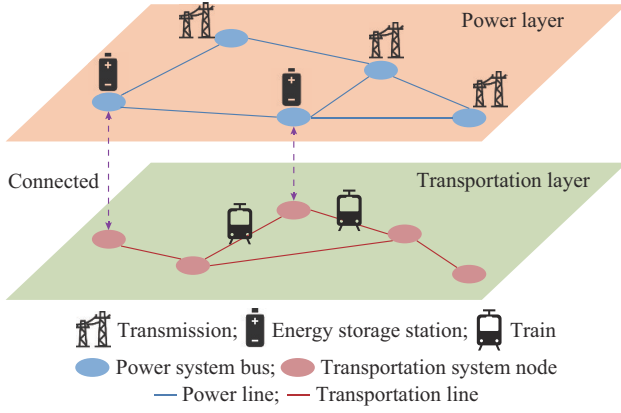


Fig. 2. Decision-making framework of decomposed problem.

B. Decomposition of Coordinated Scheduling Model of Transportation and Power Systems

In the coordinated scheduling model, the only coupling variable between the transportation and power layers is $L_{ii,v,t}$. This variable plays an important role in MESSs. To decompose the coordinated scheduling problem into two subproblems, we introduce an auxiliary variable $\tilde{L}_{ii,v,t}$, which indicates that a train is connected to the energy storage station. We add three new constraints to the coordinated scheduling model, which are expressed as:

$$\tilde{L}_{ii,v,t} = L_{ii,v,t} \lambda_{ii,v,t} \quad \forall i, \forall v, \forall t \quad (37)$$

$$\sum_{i \in \Phi^S} \tilde{L}_{ii,v,t} \leq 1 \quad \forall i, \forall v, \forall t \quad (38)$$

$$-1 \leq \sum_{ii \in \Phi^S} (\tilde{L}_{ii,v,t+1} - \tilde{L}_{ii,v,t})^2 \leq 1 \quad \forall i, \forall v, \forall t \quad (39)$$

where $\lambda_{ii,v,t}$ is the Lagrangian parameter.

Formula (37) shows the coupling constraint between the transportation and power layers. Formula (38) indicates that train v at time t can only be connected to one energy storage station. Formula (39) restricts MESSs from connecting to different energy storage stations during a time span from t to $t+1$, which is infeasible for TSN models. The coupling constraint (37) is relaxed and added to the objective function (26) as follows:

$$\min \left\{ \sum_{t \in \Phi^T} \sum_{g \in \Phi^G} (C_g P_{g,t}^G + C_g^{SU} y_{g,t} + C_g^{SD} z_{g,t}) + \sum_{t \in \Phi^T} \sum_{v \in \Phi^V} \sum_{ij \in \Phi^P} C_{ij} L_{ij,v,t} + \sum_{t \in \Phi^T} \sum_{v \in \Phi^V} \sum_{ii \in \Phi^S} \lambda_{ii,v,t} (\tilde{L}_{ii,v,t} - L_{ii,v,t}) \right\} \quad (40)$$

Therefore, the main problem (40) can be decomposed into two independent subproblems with related constraints as follows.

1) Power-layer Subproblem

$$\left\{ \begin{array}{l} \min \left\{ \sum_{t \in \Phi^T} \sum_{g \in \Phi^G} (C_g P_{g,t}^G + C_g^{SU} y_{g,t} + C_g^{SD} z_{g,t}) + \sum_{t \in \Phi^T} \sum_{v \in \Phi^V} \sum_{ii \in \Phi^S} \lambda_{ii,v,t} \tilde{L}_{ii,v,t} \right\} \\ \text{s.t. (5)-(25), (27)-(39)} \end{array} \right. \quad (41)$$

2) Transportation-layer Subproblem

$$\left\{ \begin{array}{l} \min \left\{ \sum_{t \in \Phi^T} \sum_{v \in \Phi^V} \sum_{ij \in \Phi^P} C_{ij} L_{ij,v,t} - \sum_{t \in \Phi^T} \sum_{v \in \Phi^V} \sum_{ii \in \Phi^S} \lambda_{ii,v,t} L_{ii,v,t} \right\} \\ \text{s.t. (1)-(4)} \end{array} \right. \quad (42)$$

We define x and $\varphi_1(x, \lambda)$ as the decision variables and objective function of the transportation layer, and y and $\varphi_2(y, -\lambda)$ as the decision variables and objective function of the power layer. Therefore, the dual problem (DP) is proposed as follows:

$$\max_{x,y} \inf (\varphi_1(x, \lambda) + \varphi_2(y, -\lambda)) \quad (43)$$

The objective function (43) is a nondifferentiable function. Therefore, a subgradient method is used to update the Lagrangian multiplier in this paper.

C. Improved Lagrangian Multiplier Selection

The subgradient method updates variables through the direction of its negative subgradient. The power-layer solution determines the increase or decrease of battery energy storage capacity and the charge or discharge of each energy storage station. The transportation-layer solution guarantees the minimum transportation cost, while also ensuring the power-layer solution and its constraint. The Lagrangian multiplier (transportation price indicator) coordinates the two subproblems to achieve the final results for the coordinated scheduling problem. Therefore, the subgradient of DP should not be the subgradient of individual optimal variables; rather, it should represent the subgradient of the transportation route of MESSs, which is a vector of variables. In this paper, we use the following method to calculate the subgradient of DP [23].

If $\tilde{L}_{ii,v,t} \neq L_{ii,v,t}$ update Lagrangian multiplier with (44).

$$\lambda_{ii,v,t}^{k+1} = \lambda_{ii,v,t}^k + \delta^k (\tilde{L}_{ii,v,t} - L_{ii,v,t}) \quad (44)$$

$$\delta^k = \min \left\{ C_{ij}, \mu \frac{UB - LB}{\sum_{t \in \Phi^T} \sum_{v \in \Phi^V} \sum_{ii \in \Phi^S} |\tilde{L}_{ii,v,t} - L_{ii,v,t}|} \right\} \quad (45)$$

where the superscript k is the number of iterations; UB and LB are the upper bound and lower bound in each iteration, respectively; δ^k is the step size in each iteration; and μ is the step parameter. When the number of iterations is greater than 10, μ is halved to prevent oscillations.

If $\tilde{L}_{ii,v,t} = L_{ii,v,t}$ the Lagrangian multiplier will not be updated. Essentially, the Lagrangian multiplier that does not satisfy constraint (38) is updated. During the iteration process, the program will maintain a route set (RS).

D. Calculation Process

According to the description in the previous subsections, the calculation process of the proposed algorithm is as follows.

Step 1: initialization. Set $k=0$, $\lambda_{ii,v,t}^k=0$, $RS=\emptyset$, $UB=+\infty$, $LB=-\infty$, $\mu=2$.

Step 2: $k=k+1$.

Step 3: subproblem solution. Use the given Lagrangian multiplier to solve the power-layer subproblem $\varphi_1^k(x, \lambda)$ and

the transportation-layer subproblem $\phi_2^k(y, -\lambda)$ simultaneously or sequentially. Make $f_L^k(x, y, \lambda) = \phi_1^k(x, \lambda) + \phi_2^k(y, -\lambda)$ and set $LB = f_L^k(x, y, \lambda)$ if $f_L^k(x, y, \lambda) > LB$.

Step 4: objective function update. There are two situations where the transportation-layer result can represent a feasible route. If the transportation-layer result belongs to RS , UB will not change. Otherwise, it means a new feasible transportation route will be generated. Fix the binary variable value $L_{ii,v,t}$ in the original problem as the result of the transportation-layer subproblem, and then mark it as $f^k(x, y, L_{ij})$. UB will change to $UB = f^k(x, y, L_{ij})$ if $f^k(x, y, L_{ij}) < UB$.

Step 5: convergence check. Three stopping standards are proposed in the solution procedure: ① $k > k_{\max}$; ② $(UB - LB)/UB < \varepsilon$; and ③ RS is unchanged for two consecutive iterations. k_{\max} is the maximum number of iterations. ε is the iteration accuracy.

Step 6: if one of the three convergence criteria is met, the algorithm is terminated. Otherwise, update Lagrangian multipliers and go to *Step 2*, and when $k > 10$, μ is halved.

VI. CASE STUDIES

In this section, the modified IEEE 30- and 118-bus power systems are used to demonstrate the feasibility of the proposed coordinated scheduling model and compare the economics of MESs and SESs. The proposed model is implemented in the YALMIP optimization toolbox using MATLAB R2020b and solved by Gurobi v9.5.2. The numerical experiments are performed on a computer with an Intel Core i7-11800H processor running at 2.30 GHz and 32 GB of RAM.

A. Case 1: Modified IEEE 30-bus Power System

1) Basic Data

In case 1, we have two trains for scheduling. We assume that the maximum energy of the train and the battery energy storage capacity are 90 MWh and 45 MW, respectively. The charging and discharging efficiency η is assumed to be 0.85. The battery coefficient σ is assumed to be 2. The modified IEEE 30-bus power system shown in Fig. 3 has 41 branches, 6 thermal power units with a total installed capacity of 335 MW on buses 1, 2, 13, 22, 23, and 27, and a wind farm with a total installed capacity of 160 MW on bus 13. Three energy storage stations are placed on buses 4, 13, and 25. The transportation system is also shown in Fig. 3, including one transition station. Therefore, the transportation time between station 1 and station 2 is 2 hours, while the transportation time between stations 1 or 2 and station 3 is 4 hours. The transportation cost C_{ij} is 10 \$/h.

Three models M1-M3 (the parameters are presented in Table II) in the same system are designed to compare the economics of MESs and SESs.

1) M1 refers to the proposed model with a total capacity of 90 MW.

2) M2 refers to a model in which SESs with the same capacity are distributed on buses 4, 13, and 15.

3) M3 refers to a model in which SESs with the same capacity are centralized on bus 10.

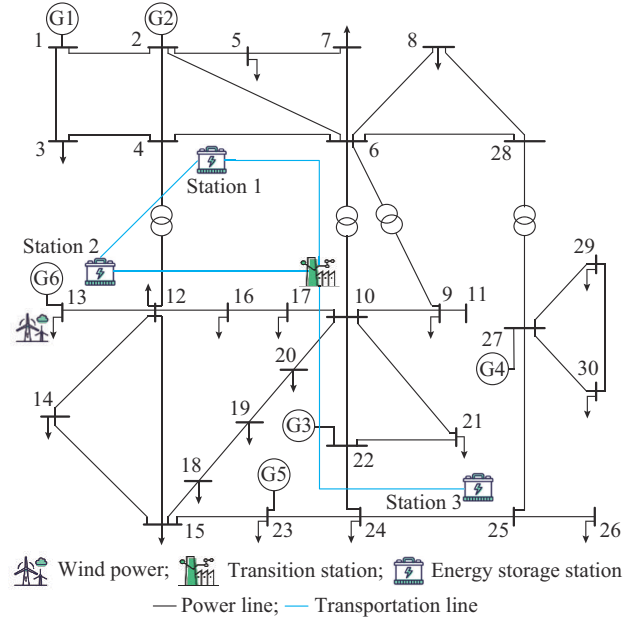


Fig. 3. Modified IEEE 30-bus power system and transportation system in case 1.

The economic value of MESs can be demonstrated by comparing M1 with M2 and M3. In addition, the economic difference between centralized and decentralized SESs can be demonstrated by a comparison of M2 and M3.

TABLE II
PARAMETERS OF MODELS M1-M3

Model	The maximum SES energy (MWh)	The maximum SES power (MW)	The maximum MES energy (MWh)	The maximum MES power (MW)
M1	60	30	90	45
M2	120	30		
M3	360	90		

To make flexible schedules, we set the initial states of energy storage stations and trains in M1 to be 50% maximum battery energy storage capacity and 25% maximum energy. The initial states of energy storage stations in M2 and M3 are 25% maximum energy. The battery energy storage capacity is equal to the sum of the battery energy storage capacity of trains and energy storage stations in M1. In other words, the total battery energy storage capacity in M1 is 90 MW, which can be exchanged between energy storage stations and trains. In M2 and M3, the battery energy storage capacities both are 90 MW, which are placed on the energy storage station and cannot be moved.

Meanwhile, to prove the peak shaving effect of energy storage in scheduling, the end states of scheduling are set the same as the initial states. In M1, the end states of trains and energy storage stations are equal to the initial states. The energy storage stations where the trains are located are also the same as the initial energy storage stations.

2) Optimal Scheduling Strategy

The battery energy storage capacity of three energy stor-

age stations and the routes of two trains during the scheduling are shown in Fig. 4. Half of the battery energy storage capacity is put on the trains at the start of the scheduling. During scheduling, the energy storage of each energy storage station is dynamically allocated through transportation. At the beginning of scheduling, due to the long distance between station 3 and other stations, the train transports the battery of station 3 to stations 1 and 2. Station 2 has a wind farm. From 05:00 to 19:00, trains transport batteries back and forth between station 1 and station 2. At 20:00, the trains return to the initial energy storage stations for charging and discharging scheduling. MESSs can provide a second method of transporting wind power in addition to transmission lines. Resource utilization in remote areas with backward facilities has been greatly enhanced. At the end of scheduling, all the trains return to the initial energy storage stations, and the battery energy storage capacity of the energy storage stations is also restored to the initial states.

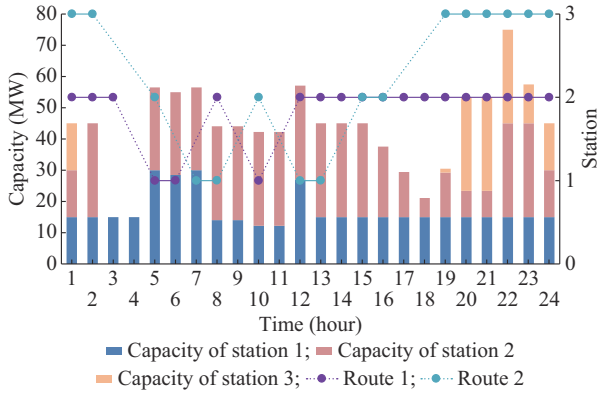


Fig. 4. Battery energy storage capacity of three energy storage stations and routes of two trains in case 1.

3) Performance of M1-M3

To evaluate the benefits of MESSs participating in power system scheduling, the results of three models are shown in Table III.

TABLE III
RESULTS OF MODELS M1-M3

Model	Operating cost (\$)	Transportation cost (\$)	R^W (%)	η^e (\$/MW)	η^u (%)
M1	14074.57	120	66.12	8.84	28.80
M2	14337.89		59.31	5.91	24.59
M3	14806.69		49.18	0.70	6.47

The wind power utilization rate R^W , energy storage economic indicator η^e , and energy storage utilization indicator η^u are expressed as:

$$R^W = \frac{\sum_{t \in \Phi^T} \sum_{i \in \Phi^S} P_{r,t}^R}{\sum_{t \in \Phi^T} P_{\max,t}^R} \times 100\% \quad (46)$$

$$\eta^e = \frac{|f(C_{\max}) - f(0)|}{C_{\max}} \quad (47)$$

$$\eta^u = \frac{\sum_{t \in \Phi^T} \sum_{i \in \Phi^S} (P_{i,t}^{cha} + P_{i,t}^{dis})}{TC_{\max}} \times 100\% \quad (48)$$

where $f(0)$ and $f(C_{\max})$ are the objective function values when the energy storage capacity is 0 and C_{\max} , respectively. The wind power utilization rate R^W represents the expected degree of wind power consumption during scheduling. The energy storage economic indicator η^e can be observed as the contribution of 1 MW increase of energy storage capacity and MESSs or SESs to the reduction of operating costs under the same conditions. The energy storage utilization indicator η^u indicates the utilization rate of all energy storage batteries during scheduling. Obviously, the values of all three indicators in M1 are higher than those of M2 and M3.

The energy and power utilization of battery energy storage in three models are shown in Fig. 5. A positive number indicates discharging, and a negative number indicates charging. The energy of M2 is larger than that of M1 from 06:00 to 15:00. The reason is the line congestion, which leads to energy redundancy. Compared with M2, the power curve of M1 is smoother. The power of M3 is significantly lower than that of M1 and M2. Therefore, the utilization of centralized SESs is much lower than that of MESSs and decentralized SESs.

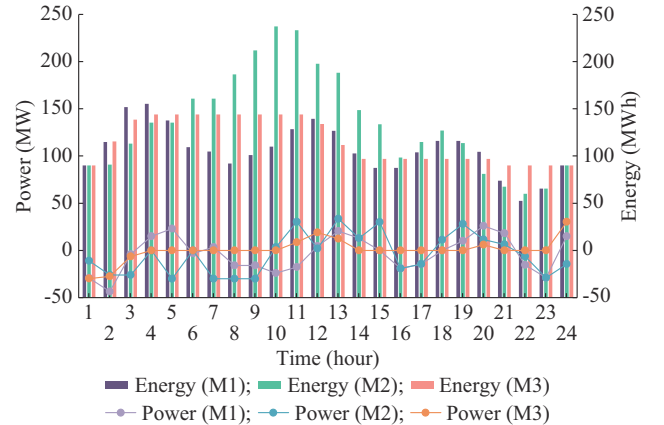


Fig. 5. Energy and power utilization of battery energy storage in three models.

4) Impact of Transportation Cost and Transmission Capacity

The operating costs and transportation time of M1 with increasing transportation cost are shown in Fig. 6.



Fig. 6. Operating costs and transportation time of M1 with increasing transportation cost.

As the transportation cost per hour increases, the transportation time decreases. According to Table III and Fig. 6, when the transportation cost exceeds 50 \$/h, the operating cost of M1 is higher than that of M2, and the transportation duration is 2 hours. However, the generation cost does not change, indicating that there are no better routes to choose. When the transportation cost reaches 125 \$/h, the trains stop running. This indicates that the transportation cost is too high, and the MESs will remain at the energy storage station as SESs. Therefore, reducing transportation cost is the key to the future application of transportation and power systems.

The impact of transmission capacity of line 12-13 (from bus 12 to bus 13) on M1 and M2 is shown in Fig. 7. The reason for selecting line 12-13 is that it is a key transmission line for wind power. The transmission capacity percent represents the percentage of the maximum transmission capacity $P_{L,max}^L$. The operating cost of M2 increases more than that of M1 with the decrease of transmission capacity. This is because the power can only be transmitted by transmission lines in M2, while the transmission method of M1 includes both MESs and transmission line. For M2, the decrease of transmission capacity leads to a large increase in wind power utilization rate. However, the decrease of the wind power utilization rate is not obvious in M1 based on MESs.

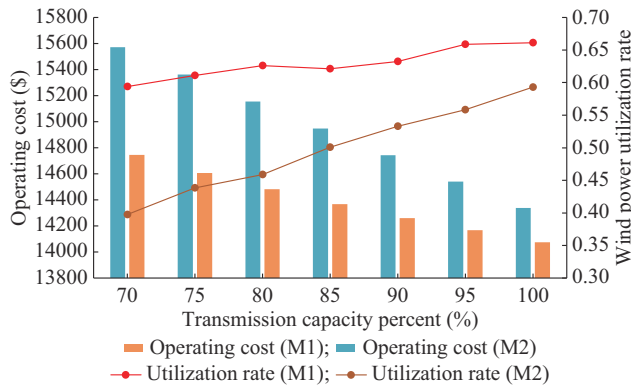


Fig. 7. Impact of transmission capacity of line 12-13 on M1 and M2.

It is obvious that MESs are a supplement to transmission lines to strengthen the transmission of renewable energy. In contrast to transmission lines, the proposed MES sharing approach can simultaneously affect multiple congestion areas and has a higher potential utilization. Moreover, the construction of a new transmission system may take several years. MESs can be deployed much more quickly when new congestion occurs due to the transmission of renewable energy in remote areas. Besides, during the construction of transmission systems, MESs can connect multiple systems to adapt to short-term changes in renewable energy resources and load demands. The case of California, USA proposed in [31] demonstrates that utility-scale MESs can alleviate congestions. In summary, the advantages of the proposed approach are as follows.

For the power systems, the proposed approach can reduce the renewable energy curtailment in areas with outdated facilities, and delay the expensive reinforcement costs brought

by newly-built transmission systems. In addition, investment in system flexibility can be reduced and the economy of the power systems can be improved.

For the renewable energy owners, the proposed approach provides new commercial opportunities. Renewable energy plants can sell more energy to customers to earn additional profits.

For energy storage operators, the proposed approach provides a new commercial model. Due to its temporal-spatial flexibility, the model provides many potential applications that SESs cannot match.

B. Case 2: Modified IEEE 118-bus Power System

1) Basic Data

We assume that the maximum energy of the train and the battery energy storage capacity are 400 MWh and 200 MW, respectively. The modified IEEE 118-bus power system has 186 branches, 54 thermal power units with a total installed capacity of 9966 MW, and a wind farm with a total installed capacity of 634 MW on bus 117. Four energy storage stations are placed on buses 25, 38, 77, and 117, which are denoted as stations 1-4. The transportation cost C_{ij} is 200 \$/h, and the transportation time for any two energy storage stations is 3 hours, which is different from those of case 1. The rest parameters and the initial and final states are the same as in case 1.

Like case 1, three models M4-M6 are compared in case 2, and the parameters are presented in Table IV.

1) M4 refers to the proposed model with a total capacity of 400 MW.

2) M5 refers to a model in which SESs with the same capacity are distributed on buses 25, 38, 77, and 117.

3) M6 refers to a model in which SESs with the same capacity are centralized on bus 117.

TABLE IV
PARAMETERS OF MODELS M4-M6

Model	The maximum SES energy (MWh)	The maximum SES power (MW)	The maximum MES energy (MWh)	The maximum MES power (MW)
M4	200	100	400	200
M5	400	100		
M6	1600	400		

2) Performance of M4-M6

The results of models M4-M6 are shown in Table V. In this case, the economic indicator of M4 is more than 400% that of M5. In Fig. 8, battery energy storage capacity in energy storage stations and the routes of two trains are presented. In contrast to case 1, case 2 cannot traverse all energy storage stations during scheduling. Two trains go back and forth between station 4 and station 2 to alleviate congestion and increase the wind power utilization rate.

3) Impact of Transportation Cost in IEEE 118-bus Power System

The operating cost and transportation time of M4 with increasing transportation costs are shown in Fig. 9.

TABLE V
RESULTS OF MODELS M4-M6

Model	Operating cost (\$)	Transportation cost (\$)	R^w (%)	η^e (\$/MW)	η^u (%)
M4	3.99×10^6	4800	34.75	102.13	27.72
M5	4.02×10^6		20.70	25.33	10.89
M6	4.03×10^6		19.91	0	7.18

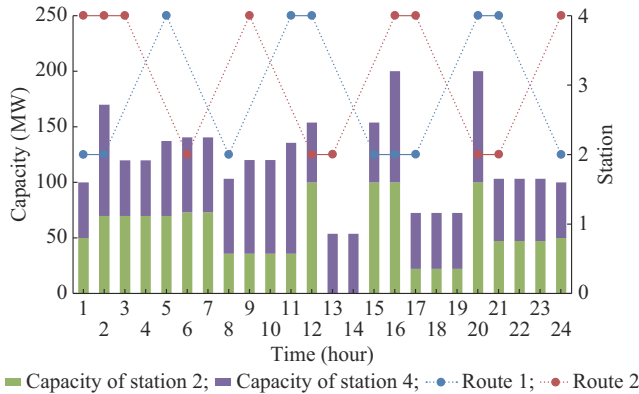


Fig. 8. Battery energy storage capacity of energy storage stations and routes of two trains in case 2.

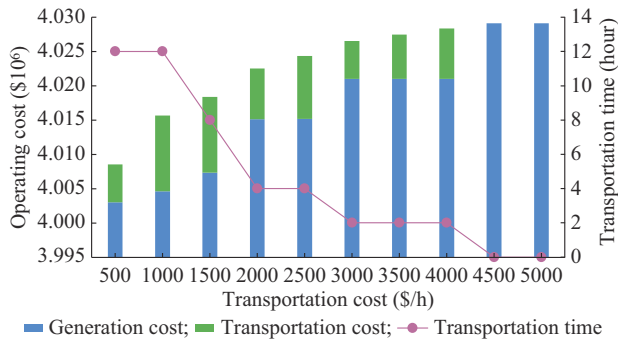


Fig. 9. Operating costs and transportation time of M4 with increasing transportation cost.

The transportation time decreases as the transportation cost increases. When the transportation cost is more than 4000 \$/h, the operating cost of M4 is more than that of M5. In general, the trend of M4 is the same as that of M1. It is demonstrated that in a large-scale power system, transportation costs also have an impact on the operating cost.

C. Performance of Proposed Algorithm

The changes of the upper and lower bounds of the proposed algorithm in case 1 are shown in Fig. 10. In the first two iterations, the upper and lower bounds have not changed, so they are not shown. The proposed algorithm is terminated by 33 iterations under the specified end conditions. *LB* represents the relaxation solution of the original problem in iteration, which cannot be realized in practice. *UB* is the optimal solution of the original problem after the transportation route is fixed. The comparison between the proposed algorithm and the centralized algorithm is shown in Table VI. The error between the results of the proposed al-

gorithm and the centralized algorithm is about 0.1% in different scale problems.

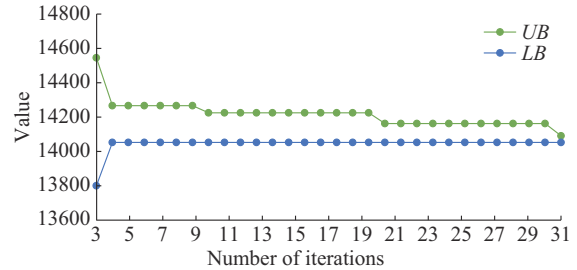


Fig. 10. Changes of upper and lower bounds of proposed algorithm in case 1.

TABLE VI
COMPARISON BETWEEN PROPOSED ALGORITHM AND CENTRALIZED ALGORITHM

Algorithm	Model	Operating cost (\$)
Proposed	M1	14090.17
Centralized	M1	14074.57
Proposed	M4	4000000.00
Centralized	M4	3990000.00

In practice, the significance of the proposed algorithm is to facilitate the coordination of optimization between two organizations with the minimum information interaction. According to (44) and (45), the iterative process of the proposed algorithm is essentially a game between power system suppliers and energy storage service providers on the train moving route. The power system suppliers hope that the trains can better allocate the location of energy storage according to the demand and reduce the operating cost of the power systems. The energy storage service providers hope to move more efficiently to decrease transportation costs.

VII. CONCLUSION

In this paper, an MES sharing approach is proposed toward system-wide temporal-spatial flexibility enhancement. A coordinated scheduling model for transportation and power systems is formulated to minimize the overall operating costs. To address the information asymmetry between transportation and power systems, a decentralized algorithm based on an improved OCD algorithm is proposed to decompose the original optimization problem. Additionally, the algorithm also enhances computational efficiency. Two cases are designed to illustrate the feasibility of the proposed coordinated scheduling model. The computational performance of the proposed algorithm is discussed in the case study as well.

Case studies demonstrate that: ① compared with decentralized SESs and centralized SESs, MESs have significantly enhanced the economic indicators and utilization indicators of energy storage; ② the proposed model has sufficient feasibility in large-scale power grids; and ③ with the decrease of transportation cost, the effect of MESs on the cost decrease of the transportation and power systems becomes

more obvious.

As for the future work, three issues deserve an in-depth study. ① Only operating costs of the transportation and power systems based on MES sharing are discussed in this paper. Future work should involve the long-term or capital costs of the proposed approach. Additionally, the specific profit model of the transportation system is also not discussed in this paper. ② In this paper, uncertainties such as congestion and breakdowns are not considered in the transportation system. The complexity of the transportation system needs to be strengthened. ③ In addition to reducing the operating cost of the transportation and power systems, another role of MESs is to enhance the resilience of power systems amidst extreme cases. In the future, operating strategies amidst extreme cases should be proposed.

REFERENCES

- [1] Y. Yu, J. Wang, Q. Chen *et al.*, “Decarbonization efforts hindered by China’s slow progress on electricity market reforms,” *Nature Sustainability*, vol. 6, pp. 1006-1015, Apr. 2023.
- [2] J. Wang, H. Zhong, Z. Yang *et al.*, “Exploring the trade-offs between electric heating policy and carbon mitigation in China,” *Nature Communications*, vol. 11, p. 6054, Nov. 2020.
- [3] J. Zhao, A. Arefi, A. Borghetti *et al.*, “An optimization model for reliability improvement and cost reduction through EV smart charging,” *Journal of Modern Power Systems and Clean Energy*, vol. 12, no. 2, pp. 608-620, Mar. 2024.
- [4] J. Han, J. Wang, Z. He *et al.*, “Hydrogen-powered smart grid resilience,” *Energy Conversion and Economics*, vol. 4, no. 2, pp. 89-104, Apr. 2023.
- [5] J. Song, G. He, J. Wang *et al.*, “Shaping future low-carbon energy and transportation systems: digital technologies and applications,” *iEnergy*, vol. 1, no. 3, pp. 285-305, Sept. 2022.
- [6] X. Li and S. Wang, “A review on energy management, operation control and application methods for grid battery energy storage systems,” *CSEE Journal of Power and Energy Systems*, vol. 7, no. 5, pp. 1026-1040, Sept. 2021.
- [7] H. Shin and J. Hur, “Optimal energy storage sizing with battery augmentation for renewable-plus-storage power plants,” *IEEE Access*, vol. 8, pp. 187730-187743, Oct. 2020.
- [8] International Energy Agency. (2024, Apr.). Batteries and secure energy transitions: world energy outlook special report. [Online]. Available: <https://www.iea.org/reports/batteries-and-secure-energy-transitions>
- [9] Clean Energy Expo. (2023, Jul.). What is energy storage on the generation side? [Online]. Available: https://www.sohu.com/a/696718074_120008270
- [10] J. Wang, Q. An, Y. Zhao *et al.*, “Role of electrolytic hydrogen in smart city decarbonization in China,” *Applied Energy*, vol. 336, p. 120699, Apr. 2023.
- [11] C. Yin, J. Wang, W. Tang *et al.*, “Health-aware energy management strategy toward Internet of storage,” *IEEE Internet of Things Journal*, vol. 10, no. 9, pp. 7545-7553, May 2023.
- [12] C. Zhang, Y. Yang, X. Liu *et al.*, “Mobile energy storage technologies for boosting carbon neutrality,” *The Innovation*, vol. 4, no. 6, p. 100518, Nov. 2023.
- [13] Fortune Business Insights. (2024, Jan.). Mobile energy storage system market size. [Online]. Available: <https://www.fortunebusinessinsights.com/mobile-energy-storage-system-market-105656>
- [14] Massachusetts Department of Energy Resource. (2020, Feb.). Mobile energy storage study: emergency response and demand reduction. [Online]. Available: <https://www.mass.gov/doc/doer-executive-summary-mobile-energy-storage-study>
- [15] A. Ali, H. H. Mousa, M. F. Shaaban *et al.*, “A comprehensive review on charging topologies and power electronic converter solutions for electric vehicles,” *Journal of Modern Power Systems and Clean Energy*, vol. 12, no. 3, pp. 675-694, May 2024.
- [16] Nomad Transportable Power Systems. (2023, May). The future of energy is mobile. [Online]. Available: <https://www.fortunebusinessinsights.com/mobile-energy-storage-system-market-105656>
- [17] J. Ma, H. Kong, J. Wang *et al.*, “Carbon-neutral pathway to mitigating transport-power grid cross-sector effects,” *The Innovation*, vol. 5, no. 3, p. 100611, May 2024.
- [18] G. Kim, Y. S. Ong, C. K. Heng *et al.*, “City vehicle routing problem (city VRP): a review,” *IEEE Transactions on Intelligent Transportation Systems*, vol. 16, no. 4, pp. 1654-1666, Aug. 2015.
- [19] H. Niu and X. Zhou, “Optimizing urban rail timetable under time-dependent demand and oversaturated conditions,” *Transportation Research Part C: Emerging Technologies*, vol. 36, pp. 212-230, Nov. 2013.
- [20] L. Yang and X. Zhou, “Constraint reformulation and a Lagrangian relaxation-based solution algorithm for a least expected time path problem,” *Transportation Research Part B: Methodological*, vol. 59, pp. 22-44, Jan. 2014.
- [21] H. Saboori and S. Jadid, “Optimal scheduling of mobile utility-scale battery energy storage systems in electric power distribution networks,” *Journal of Energy Storage*, vol. 31, p. 101615, Oct. 2020.
- [22] Y. Sun, Z. Li, M. Shahidehpour *et al.*, “Battery-based energy storage transportation for enhancing power system economics and security,” *IEEE Transactions on Smart Grid*, vol. 6, no. 5, pp. 2395-2402, Sept. 2015.
- [23] Y. Sun, Z. Li, W. Tian *et al.*, “A Lagrangian decomposition approach to energy storage transportation scheduling in power systems,” *IEEE Transactions on Power Systems*, vol. 31, no. 6, pp. 4348-4356, Nov. 2016.
- [24] Y. Sun, J. Zhong, Z. Li *et al.*, “Stochastic scheduling of battery-based energy storage transportation system with the penetration of wind power,” *IEEE Transactions on Sustainable Energy*, vol. 8, no. 1, pp. 135-144, Jan. 2017.
- [25] W. Sun, W. Liu, J. Zhang *et al.*, “Bi-level optimal operation model of mobile energy storage system in coupled transportation-power networks,” *Journal of Modern Power Systems and Clean Energy*, vol. 10, no. 6, pp. 1725-1737, Nov. 2022.
- [26] X. Liu, C. B. Soh, T. Zhao *et al.*, “Stochastic scheduling of mobile energy storage in coupled distribution and transportation networks for conversion capacity enhancement,” *IEEE Transactions on Smart Grid*, vol. 12, no. 1, pp. 117-130, Jan. 2021.
- [27] M. Zhou, Z. Wu, J. Wang *et al.*, “Forming dispatchable region of electric vehicle aggregation in microgrid bidding,” *IEEE Transactions on Industrial Informatics*, vol. 17, no. 7, pp. 4755-4765, Jul. 2021.
- [28] Z. Wang, J. Gao, R. Zhao *et al.*, “Optimal bidding strategy for virtual power plants considering the feasible region of vehicle-to-grid,” *Energy Conversion and Economics*, vol. 1, no. 3, pp. 238-250, Dec. 2020.
- [29] J. Kim and Y. Dvorkin, “Enhancing distribution system resilience with mobile energy storage and microgrids,” *IEEE Transactions on Smart Grid*, vol. 10, no. 5, pp. 4996-5006, Sept. 2019.
- [30] X. Jiang, J. Chen, Q. Wu *et al.*, “Two-step optimal allocation of stationary and mobile energy storage systems in resilient distribution networks,” *Journal of Modern Power Systems and Clean Energy*, vol. 9, no. 4, pp. 788-799, Aug. 2021.
- [31] G. He, J. Michalek, S. Kar *et al.*, “Utility-scale portable energy storage systems,” *Joule*, vol. 5, no. 2, pp. 379-392, Feb. 2021.
- [32] H. Hayajneh and X. Zhang, “Logistics design for mobile battery energy storage systems,” *Energies*, vol. 13, no. 5, p. 1157, Mar. 2020.
- [33] J. Yan, F. Lai, Y. Liu *et al.*, “Multi-stage transport and logistic optimization for the mobilized and distributed battery,” *Energy Conversion and Management*, vol. 196, pp. 261-276, Sept. 2019.
- [34] T. Liu, P. Wang, Q. Peng *et al.*, “Operation-area-constrained adaptive primary frequency support strategy for electric vehicle clusters,” *Journal of Modern Power Systems and Clean Energy*, vol. 11, no. 6, pp. 1982-1994, Nov. 2023.
- [35] Y. Li and Y. Han, “A module-integrated distributed battery energy storage and management system,” *IEEE Transactions on Power Electronics*, vol. 31, no. 12, pp. 8260-8270, Dec. 2016.
- [36] J. Wang, H. Zhong, Z. Yang *et al.*, “Incentive mechanism for clearing energy and reserve markets in multi-area power systems,” *IEEE Transactions on Sustainable Energy*, vol. 11, no. 4, pp. 2470-2482, Oct. 2020.

Yuhang Ding received the B.S. degree in electrical engineering from Hangzhou Dianzi University, Hangzhou, China, in 2020, and the M.S. degree in electrical engineering from North China Electric Power University, Beijing, China, in 2023. He is currently working in State Grid Hangzhou Lin’an District Power Supply Company, Hangzhou, China. His research interests include power system optimization and mobilized energy storage.

Xinjiang Chen received the B.S. degree in traffic engineering from Wuyi

University, Jiangmen, China, in 2018, and the M.S. degree in transportation engineering from Central South University, Changsha, China, in 2021. He is currently pursuing the Ph.D. degree in College of Engineering, Peking University, Beijing, China. His current research interests include computational intelligence, and energy and transportation system optimization.

Guangchun Ruan received the Ph.D. degree in electrical engineering from Tsinghua University, Beijing, China, in 2021. He is currently a Post-doctor with the Laboratory for Information & Decision Systems (LIDS) at Massachusetts Institute of Technology (MIT), Cambridge, USA. Before joining MIT, he was a Post-doctor with the University of Hong Kong, Hong Kong, China, in 2022, a Visiting Scholar with Texas A&M University, Texas, USA, in 2020, and a Visiting Scholar with the University of Washington, Washington, USA, in 2019. His research interests include electricity market, energy resilience, demand response, data science, and machine learning application.

Gengyin Li received the B.S., M.S., and Ph.D. degrees from North China Electric Power University, Beijing, China, in 1984, 1987, and 1996, respectively, all in electrical engineering. Since 1987, he has been with the School of Electrical and Electronic Engineering, North China Electric Power University, where he is currently a Professor. His research interests include high-voltage direct current (HVDC) transmission, power quality analysis and control, and emerging transmission and distribution technology.

Ming Zhou received the B.S., M.S., and Ph.D. degrees in electrical engineering from North China Electric Power University, Beijing, China, in 1989, 1992, and 2006, respectively. Since 1992, she has been with the School of Electrical and Electronic Engineering, North China Electric Power University, where she is currently a Professor. Her research interests include power system economics, HVDC transmission, electricity market, and power quality analysis.

Dai Jiang received the B.Eng. degree from the College of Automation, Kunming University of Science and Technology, Kunming, China, in 2008, and the M.Eng. degree from the College of Electrical Engineering, Chongqing University, Chongqing, China, in 2011. He is currently working as a Senior Engineer in Power Dispatching and Controlling Center of Guizhou Power Grid Company Limited, Guizhou, China. His research interests include power dispatching operation analysis and control.

Jianxiao Wang received the B.S. and Ph.D. degrees in electrical engineering from Tsinghua University, Beijing, China, in 2014 and 2019, respectively. He was a Visiting Student Researcher at Stanford University, Stanford, USA. He is currently an Assistant Professor with Peking University, Beijing, China. His research interests include data-driven decision making for smart grid and energy storage.